Influence of simple fracture intersections with differing aperture on density-driven immiscible flow: Wetting versus nonwetting flows

Sung-Hoon Ji,[1] Michael J. Nicholl,[2] Robert J. Glass,[3] and Kang-Kun Lee[4]

Received 7 February 2006; revised 13 June 2006; accepted 24 July 2006; published 13 October 2006.

[1] We conducted laboratory experiments to evaluate the effects of simple fracture intersections with differing aperture on density-driven immiscible wetting (water into air) and nonwetting (Trichloroethylene into water) flows, and analyzed them quantitatively. The experimental systems consisting of vertical and horizontal fractures were fabricated with glass for easy visualization. The aperture variation between intersecting fractures and the viscous force of the injected fluid were considered to be critical system parameters. Experimental results show the critical difference between the wetting and nonwetting flows by the intersection and viscous force, and subsequent mathematical analyses explain well our observations: The intersection acts as a capillary barrier (CB) for the wetting and capillary bridge for the nonwetting flows, and the viscous force of flowing fluids reduces the strength of CBs. The results of both laboratory experiments and mathematical analyses suggest that the fracture intersection with differing aperture can be a more significant factor controlling the network-scale phase structure for the nonwetting than the wetting flows.

Citation: Ji, S.-H., M. J. Nicholl, R. J. Glass, and K.-K. Lee (2006), Influence of simple fracture intersections with differing aperture on density-driven immiscible flow: Wetting versus nonwetting flows, *Water Resour. Res.*, *42*, W10416, doi:10.1029/2006WR004953.

1. Introduction

[2] Multiphase flow in fractured rocks has received considerable attention for its application fields such as radioactive waste disposal and nonaqueous phase liquid (NAPL) originated subsurface contamination. In particular, the phase structure is a primary concern because it determines the pressure-saturation-conductivity relation and the solute transport pattern in fractured rocks. The void space of a fracture network is composed of individual fractures and the intersections between those fractures. The geometry of the intersections will differ from that of the contributing fractures, thus introducing heterogeneities that are well-connected and span the network in three dimensions. An abrupt change in void geometry between fracture and intersection will perturb the balance between capillary, gravitational, viscous, and inertial forces that controls multiphase immiscible flow and thus the phase structure. This is particularly important with respect to capillary forces, where a change in void geometry can lead to the formation of a capillary barrier (CB), or alternatively a conduit. On the basis of capillary considerations alone, a sudden increase in void size could act as a barrier to wetting phase flow or draw in nonwetting phase flow, with the opposite effects for a decrease in void size. In addition to change in void size, the work required for menisci to navigate corners will also factor into the formation of barriers or conduits at fracture intersections.

[3] Recent experiments designed to explore unsaturated flow in fracture networks support the idea that CBs formed at fracture intersections can be a critical control factor on the behavior of the flow. A simple field experiment in a natural fracture network suggested that fracture intersections could both focus and fragment an infiltrating fluid slug [*Glass et al.*, 2002a; *Nicholl and Glass*, 2002]. The controlling influence of fracture intersections has also been inferred from laboratory experiments considering unsaturated flow in two-dimensional networks of water-wettable vertical and horizontal fractures. Fracture intersections were believed to be responsible for temporal fluctuations in outflow and internal pathway switching that were observed over an ~18-month period of steady supply to a point source located at the top of a ~2-m-tall analog fracture-matrix network [*Glass et al.*, 2002b]. In other fracture-matrix networks of similar geometry, application of water to sources distributed along the upper boundary led to pathway switching and large-scale confluencing of flow that were also attributed to fracture intersections [*LaViolette et al.*, 2003; *Wood et al.*, 2004]. Intersections terminating in a vertical fracture have been found to keep flow structures narrow and focused [*Glass et al.*, 2003].

[4] The ability of a single intersection to impose spatial and temporal structure on unsaturated (wetting phase) flow

[1]Department of Earth Sciences, University of Waterloo, Waterloo, Ontario, Canada.
[2]Geoscience Department, University of Nevada, Las Vegas, Nevada, USA.
[3]Flow Visualization and Processes Laboratory, Sandia National Laboratories, Albuquerque, New Mexico, USA.
[4]School of Earth and Environmental Sciences, Seoul National University, Seoul, South Korea.

0043-1397/06/2006WR004953$09.00

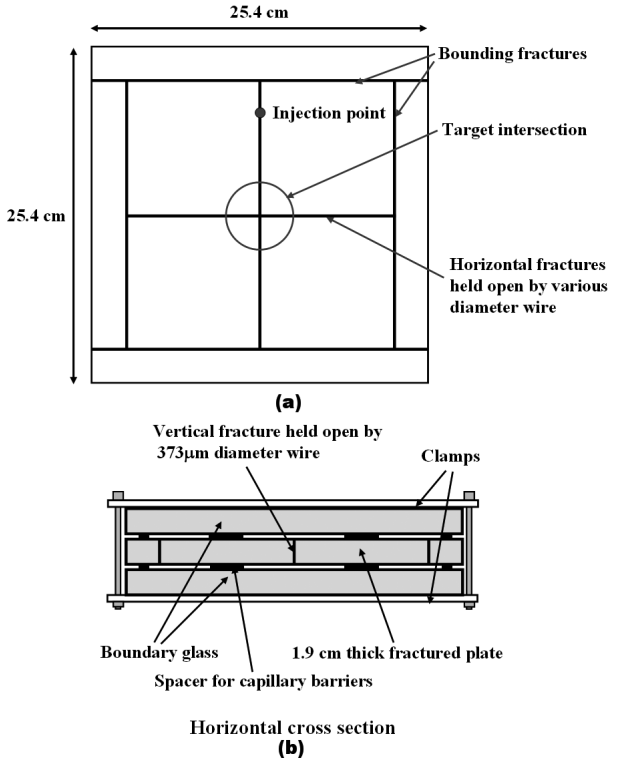

Figure 1. Conceptual drawing of the model intersection: (a) side view and (b) cross section.

was considered by *Wood et al.* [2002, 2005]. They assembled intersections between constant aperture (0.07 cm) vertical and horizontal fractures and observed the changes in unsaturated flow across each intersection as the supply rate was decreased. For all of their intersection geometries and across a wide range of supply rates, water pooled above a CB formed at the intersection. At high flow rates, they observed an intersection-spanning fluid tendril that snapped as the supply rate was decreased. At lower flow rates, the intersection imposed a regular temporal signal by accumulating water above the barrier and then releasing a portion of the stored volume when sufficient pressure accumulated to breach the CB. Repetition of this process transformed a steady inflow into a pulsed outflow. In most cases, fluid was, at least partially, diverted into the horizontal fractures, thus providing a mechanism for confluencing and pathway switching. They also found that solid material spanning the intersection could impose a different type of temporal signal by metering flow across the point connection. In other unsaturated flow experiments, *Dragila and Weisbrod* [2004] observed mode switching between aperture-spanning and film flow as water traversed an intersection where a vertical fracture bifurcated.

[5] The influence of fracture intersections on nonwetting phase flow was first considered in a preliminary study by *Ji et al.* [2004]. A 25.4 × 25.4 × 1.9 cm glass plate was broken to create an intersection between horizontal and vertical fractures of approximately equal aperture (371 μm). For wetting phase flow (water into air) their results are consistent with those of *Wood et al.* [2002, 2005]. The intersection acted as a CB to unsaturated flow, diverting low flows into the horizontal fractures and discharging fluid at regular intervals. An intersection-spanning tendril developed as the flow was increased, and the tendril snapped to reestablish a regular discharge cycle as the flow was decreased. The same intersection model was later brought to a water-saturated condition in order to explore density-driven flow of a nonwetting phase by injecting Trichloroethene (TCE), a dense nonaqueous phase liquid (DNAPL). The result was opposite to that for unsaturated flow, and the intersection provided a negligible impediment to TCE migration. Instead, the first blob of TCE arriving at the intersection became trapped within the vertical fracture, providing a bridge across the intersection for subsequent flow. As with the wetting phase experiment, an intersection-spanning tendril of TCE formed as the supply rate was increased. However, unlike the wetting phase experiment, the TCE tendril thinned but did not snap as the supply rate was decreased.

[6] In this study, we build on the work of *Wood et al.* [2002, 2005] and *Ji et al.* [2004] to further our understanding of how fracture intersections influence two-phase flow. We designed our experiments to address open questions regarding intersections between fractures of differing aperture for both wetting and nonwetting phase flows, and analyzed them quantitatively. Given the wide range of possible fracture intersections, we choose to focus on an intersection between vertical and horizontal fractures, where the difference between capillary and gravitational forces is maximized. Following *Glass et al.* [2003] and *Ji et al.* [2004], we fabricated our test intersection by breaking a glass plate. This process produces an intersection with very well defined corners and allows observation of the flow processes within the fracture planes. We held the aperture of the vertical fracture constant and altered capillary heterogeneity at the intersection by varying the aperture of the horizontal fracture (three different horizontal apertures). For each of our three models we considered two types of density-driven immiscible flow: wetting phase flow (water into air) and nonwetting phase flow (TCE into water). In each trial the supply rate was varied over ~3 orders of magnitude, first up from zero and then back down for characterizing the viscous effects of the injected fluids. Our experimental procedure is presented in section 2, with the resulting observations in section 3. We then provide a mechanistic explanation for the observed behavior in section 4, and conclude with a short summary of our results in section 5.

2. Experimental Setup

[7] We constructed a simple intersection between vertical and horizontal fractures by inducing controlled breaks in a 25.4 × 25.4 cm plate of 1.9 cm thick glass (Figure 1). Individual fractures were created at predetermined locations by holding a strip of Nichrome™ wire against the glass, then applying direct current to heat the wire [*Glass et al.*, 2003; *Ji et al.*, 2004]. The glass plate expanded in response to the linear heat source and fractured under tension. The resulting fracture was smooth at the microscopic level with mild macroscopic undulations, including a gentle conchoidal pattern that pointed in the direction of fracture propagation and represented rhythmic arrest lines [see *Kulander et al.*, 1979; *Bahat and Engelder*, 1984]. We first induced "bounding fractures" parallel to each edge of the glass plate as a

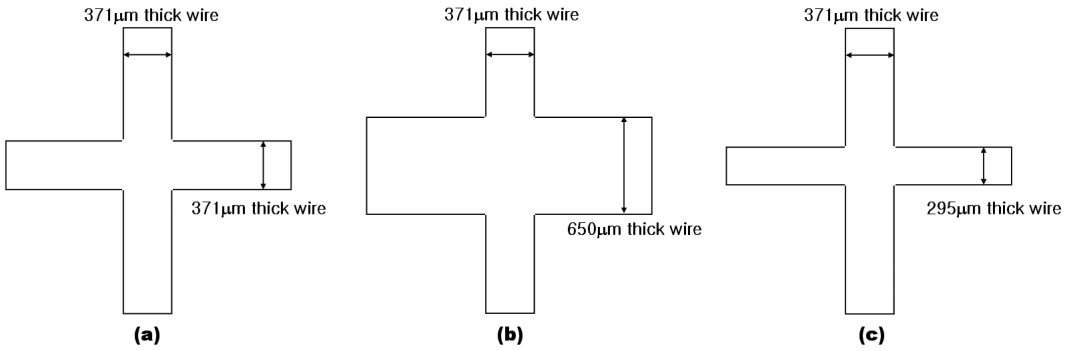

Figure 2. Approximate aperture configurations for (a) case 0, (b) case 1, and (c) case 2.

means of imposing boundary conditions (Figure 1a). To create our target intersection, the vertical fracture was induced first, then the horizontal. As a result, the vertical fracture was continuous, while the two sides of the horizontal fracture exhibited a slight mismatch (<0.1 cm) where they met at the vertical fracture. Such mismatch is expected in any situation where fracture sets are sequential rather than concurrent, and thus likely to be ubiquitous in natural systems. Finally, we note that this fracturing process is not a trivial matter, as we had to break a large number of plates in order to achieve one good fracture pattern.

[8] Each of the four fractures contributing to our target intersection (upper/lower vertical, left/right horizontal) was held open by inserting three short pieces of wire, two on one side and one on the other (Figure 1a). In order to minimize their impact on the experiment, the wire pieces were inserted a short distance (~0.1 cm) into the fracture plane and located a substantial distance (2.54 cm) away from the intersection [see *Ji et al.*, 2004]. To vary the influence of capillary forces alone, we changed the aperture of the horizontal fracture between trials and held the vertical fracture constant (Figure 2). A 371-μm-diameter wire was selected for the vertical fracture. For the horizontal fracture, we first considered an aperture equal to the vertical [e.g., *Ji et al.*, 2004] (case 0, 371 μm, Figure 2a), then larger (case 1, 650 μm, Figure 2b), and finally smaller (case 2, 295 μm, Figure 2c). The resulting apertures fall within the range of natural fractures [e.g., *Hakami and Larsson*, 1996; *Keller*, 1998; *Lee et al.*, 2003] and facilitate competition between gravity and capillary forces [*Wood et al.*, 2005]. The aperture of the bounding vertical fractures was chosen to discourage entry by the invader fluid, and thus constrain flow to our target intersection; 650 μm for wetting invasion (water to air), and 295 μm for nonwetting invasion (TCE to water). The horizontal bounding fractures were set to allow free exit by the flowing phase.

[9] The fractured glass plate was mechanically supported by clamping it between two unfractured plates of the same size (Figure 1b). Spacers were placed between the fractured plate and the supporting plates in order to create CBs, and thus constrain flow to within the fractured plate [see *Glass et al.*, 2003; *Ji et al.*, 2004]. These spacers were set at 1100 μm for wetting phase flow and 80 μm for nonwetting phase flow. For the wetting phase flow we applied deionized water dyed with 1.0 g/L of FD&C Blue #1 to an air-filled system; for the nonwetting phase flow, reagent grade TCE was dyed with 0.9 g/L of Oil-Red-O and applied to a system saturated with deionized water; see Table 1 for fluid properties. The flowing fluid (water or TCE) was applied under positive pressure to a point source in the vertical fracture at a location 7.6 cm above the intersection. In order to maintain a constant surface chemistry for the fractures, all the surfaces were thoroughly cleaned before each experiment. To avoid creating a large volume of toxic cleaning waste (e.g., concentrated sulfuric acid), we developed a complex regimen that involved separate labor intensive washes using vegetable oil, heated Alconox™ solution, and dilute ammonia. Tests showed that our process produced repeatable contact angles of ~5° (range 2° to 9°) for water-air and ~160° (range 155° to 164°) for TCE-water, which were measured from snapshots of water and TCE drops on the glass plate in air- and water-saturation conditions, respectively.

3. Experimental Results

[10] Each experiment was begun under single phase conditions (fractures were fully air or water saturated). Flow was initiated at a steady rate of 0.012 mL/min, then increased to 10 mL/min (0.012, 0.10, 0.50, 1.00, 5.00, and 10.00 mL/min) and back down to 0.012 mL/min along the same sequence. Each step lasted for the greater of 5 min or 2 mL of fluid injection. This range of supply rates was chosen to vary the influence of viscous forces across ~3 orders of magnitude. The maximum supply rate was set to be of a similar order to that expected for density-driven piston displacement (~50 mL/min) as predicted by the cubic law [e.g., *Bird et al.*, 1960]. Each experiment, repeated several times for each case, was continuously documented using a still camera and two digital video cameras, which was employed in image processing to measure pool heights at the test intersection. Experimental results for cases 0–2 (Figure 2) are presented below, first for wetting phase flow (section 3.1) then for nonwetting phase flow (section 3.2).

Table 1. Physical Properties of Experimental Fluids

Fluid	Density, g/mL	Viscosity, cP at 25°C	Interfacial Tension, mN/m
Water[a]	0.998	1.000	NA
Air[a]	0.001	0.018	73
TCE[b]	1.469	0.575	27

[a]From *Weast* [1985].
[b]From *Glass et al.* [2000].

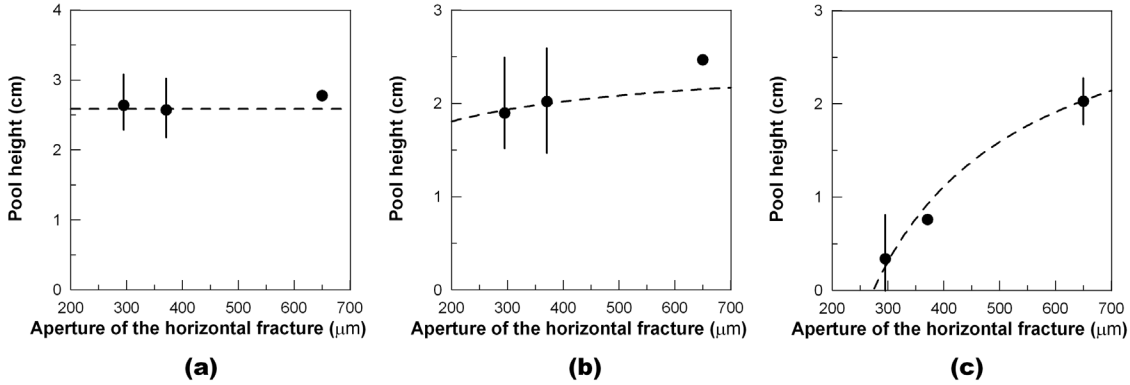

Figure 3. The relationship between the aperture of the horizontal fracture and the mean pool height (a) prior to the first entry into horizontal fractures; (b) prior to the first drainage into the lower vertical fracture; and (c) after drainage. The aperture of the vertical fracture is constant to 371 μm. The dots and solid lines are the means and ranges of observed values, respectively. The dashed lines are estimated pool heights using equations (2)–(4) and (8).

3.1. Wetting Phase Flow

[11] In case 0 (Figure 2a), the initial application of water produced a sequence of small teardrop-shaped water blobs (~0.7 cm tall × ~0.2 cm wide) in the upper vertical fracture [see *Ji et al.*, 2004]. The intersection formed a CB, causing water to be accumulated above it. This region is called a pool whose height is defined by the distance between the intersection and the peak of the convex of a pool. When the curvilinear surface of the pool reached a height of ~2.2 cm above the intersection, the initial CB breached and water drained into the right-hand horizontal fracture. Pools in the right-hand and vertical fracture became disconnected, reestablishing the CB. The pool height rose in response, and the right-hand fracture was reinvaded. The pool height rose after the right-hand fracture was full, then fell as the water entered into the left-hand fracture and released a single water blob into the lower vertical fracture. The intersection developed a regular "fill and drain" cycle after storage in the left-hand fracture was filled with a maximum pool height of ~1.4 cm and a minimum of ~0.9 cm. Unlike the experiments of *Wood et al.* [2002], the horizontal fractures did not participate in the fill and drain cycle; hence dynamic storage was limited to the upper vertical fracture. Increasing the supply rate to 0.1 mL/min led to the formation of a continuous tendril above the intersection; pool height fell from a maximum of ~1.3 cm to a minimum of ~0.9 cm when a blob was discharged from the intersection. A tendril formed below the intersection at 0.5 mL/min. Both tendrils widened as the supply rate was increased, and narrowed as it was decreased. Pulsed flow returned below the intersection at 0.1 mL/min, and above at 0.012 mL/min.

[12] In case 1 (Figure 2b), the initial application of water flowed down one surface of the vertical fracture in free-surface flow. Water pooled above the intersection to a height of ~2.7 cm and then fell to a low of ~1.4 cm as it invaded the left-hand horizontal fracture. The horizontal pool disconnected from the vertical pool, reestablishing the CB. The pool height increased to ~2.3 cm and then reinvaded the left-hand horizontal fracture. Pool height rose again when the left-hand fracture was full. At a pool height of ~2.5 cm, water was discharged into the lower vertical fracture in the form of blobs (~0.8 × ~0.7 cm). The system then settled into a regular pulsed flow regime with maximum and minimum pool heights of ~2.5 and ~2.2 cm. The right-hand horizontal fracture remained dry, and the left-hand fracture remained full during discharge. Unlike case 0, this model continued in pulsed discharge mode across ~3 orders of magnitude change in supply rate and never developed a stable tendril below the intersection.

[13] In case 2 (Figure 2c), the initial application of water flowed down one surface of the vertical fracture in free-surface flow. Water pooled above the intersection to a height of ~3.1 cm and then fell to a low of ~1.1 cm as it invaded the left-hand horizontal fracture. After filling the left-hand fracture, pool height rose to ~2.1 cm, breaching the CB and invading both the right-hand horizontal and the lower vertical fractures as pool height fell to ~0.5 cm. This split discharge continued, adding water to the right-hand fracture with each successive event. Multiple disconnected pools formed within the right-hand fracture, leading to high variability in behavior. A stable tendril formed below the intersection when the supply rate was increased to 1.00 mL/min. With the intersection open to flow, a portion of the discharge entered the right-hand fracture, eventually causing it to fill. The tendril snapped and the system returned to pulsed flow when the supply rate was decreased to 0.1 mL/min. The minimum pool height following discharge remained very low until flow was dropped to 0.012 mL/min.

[14] Figure 3a shows the relationship between the arithmetic mean of pool heights for the first invasion into the horizontal fracture and the aperture of the horizontal fractures. They were unrelated to the aperture variation of the intersecting fractures. However, the mean pool heights for the first drainage to the lower vertical fracture (Figure 3b) and after drainage (Figure 3c), were increased, as the aperture of the horizontal fracture was increased. Considering *Wood et al.* [2002, 2005] and *Ji et al.* [2004], these results suggest that there are two CBs at a simple crossed fracture intersection for the wetting invasion: The first one is related to the first invasion into the horizontal fractures and is not affected by the aperture variation of intersecting fractures, while the second one, influenced by the differing aperture of intersecting fractures, is concerned with the

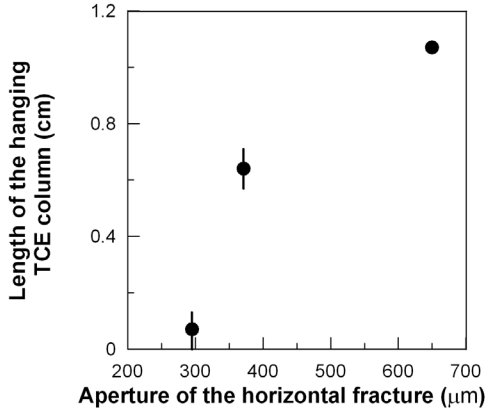

Figure 4. The relationship between the mean length of hanging TCE columns and the aperture of horizontal fractures for nonwetting flows. The aperture of the vertical fracture is maintained at constant aperture of 371 μm.

drainage into the lower vertical fracture through the intersection and the minimum pool height after breach. The response of the phase structure to increasing injection rate for each case also supports the idea that the second CB is influenced by the aperture variation of intersecting fractures: The horizontal fracture having a larger aperture than the vertical one makes the second CB difficult to breach.

3.2. Nonwetting Phase Flow

[15] In case 0 (Figure 2a), the initial application of TCE produced a sequence of medium-sized ($\sim$1.1 $\times$ $\sim$0.6 cm) blobs in the upper vertical fracture [see *Ji et al.*, 2004]. Blobs formed with a bulbous head and narrow tail, but quickly became rounded during their advance. The first blob entered the intersection and stopped. The TCE pool first grew upward and laterally, but did not fully fill the fracture in the direction orthogonal to both dip and pole vectors. Then, when the pool reached a height of 0.62 cm above the intersection, with the next drop of TCE it began to invade the lower vertical fracture and form a hanging column. However, the pool height is not particularly significant because it is more influenced by the blob size than by the entry pressure for the invasion into the lower vertical fracture. As the TCE column grew, it bifurcated below the intersection to release a fluid blob. A regular behavior developed in which the arrival of a TCE blob at the top of the pool was shortly followed by the release of a similarly sized blob from the hanging column. During this process, the pool remained pinned across the intersection, acting as a bridge between the upper and lower halves of the vertical fracture. The pool bulged slightly along both sides of the horizontal fracture but did not enter either one. A pulsing tendril developed above the intersection at a supply rate of 0.50 mL/min and stabilized at 1.00 mL/min. A stable tendril developed below the intersection at 5.00 mL/min. Both tendrils widened as the supply rate was increased. The tendrils narrowed but did not snap as the supply rate was decreased. At 0.012 mL/min, the tendrils locally narrowed to below the fracture aperture, detaching from one of the fracture walls to create a pool and thread structure. The pool bridging the intersection declined in size as the supply rate was increased, and remained small as the supply rate was decreased.

[16] In case 1 (Figure 2b), the first TCE blob ($\sim$5.6 $\times$ $\sim$0.5 cm dimension) invaded the intersection and entered both of the horizontal fractures, mostly the right-hand one. Additional blobs invaded the horizontal fractures, spreading out into disconnected pools that did not connect with the vertical fracture. The horizontal fractures did not fill until after the supply rate was increased to 0.10 mL/min. After fully filling the horizontal fractures, a complicated pool of TCE began to form above the intersection, and a few drops of TCE were released into one of the vertical bounding fractures. Release to the bounding fracture stopped in less than a minute as a hanging column developed below the intersection when pool height reached $\sim$5.5 cm, which was not related to the entry pressure but the length of TCE blobs. As in case 0, blobs were discharged from the hanging column in response to the addition of fluid from above. A stable tendril developed above the intersection at 0.50 mL/min and below the intersection at 1.00 mL/min. Formation of a continuous tendril below the intersection led to drainage of the horizontal fractures through the tendril, in contrast to the pattern of the wetting flow, due to lower viscosity of TCE than water. The horizontal fractures refilled when the supply rate was increased to 5.00 mL/min. The horizontal fractures again drained through the tendril as flow was decreased. The tendril below the intersection snapped at 0.10 mL/min, and flow was diverted into the horizontal fractures. After the horizontal fractures filled, they drained again through a tendril, and then filled again after the tendril snapped. This behavior continued as flow was decreased to 0.012 mL/min. Once formed, the tendril above the intersection remained intact.

[17] In case 2 (Figure 2c), the initial injection formed a large blob ($\sim$5.8 $\times$ $\sim$0.5 cm) of TCE that invaded the intersection and pooled above it to a height of $\sim$2.9 cm. The next blob of TCE increased the pool height to $\sim$6.3 cm and released a blob ($\sim$3.4 $\times$ $\sim$0.5 cm) into the lower vertical fracture. The horizontal fractures were not invaded by the TCE pool throughout this experiment. Unlike the other two nonwetting phase experiments, blobs were released directly from the bottom of the intersection without a hanging TCE column. A stable tendril formed above the intersection at 0.10 mL/min and below the intersection at 0.50 mL/min. The tendrils widened with increased supply rate, then narrowed but did not snap as the supply rate was decreased. As in case 0, the tendrils narrowed locally to less than the fracture aperture, detaching from one of the fracture walls.

[18] Although TCE always invaded the target intersection when the front of a TCE blob met it, we can infer the effect of aperture variation of the intersecting fractures from the different observations in all cases. First, it affected the nonwetting invasion path in a fracture network: While TCE went down to the lower vertical aperture in cases 0 and 2, it went to the horizontal fractures before draining from the test intersection in case 1. This result agrees with the estimation derived from the concept of the invadability that is defined from an invasion pressure due to local capillary, gravity, and viscous forces [*Meakin et al.*, 1992; *Xu et al.*, 1998; *Amundsen et al.*, 1999; *Ji et al.*, 2003]. Figure 4 shows the arithmetic mean of lengths of the hanging TCE columns after the first drainage into the lower vertical fracture in each case. It grew as the aperture of the horizontal fracture increased: A smaller capillary pressure in

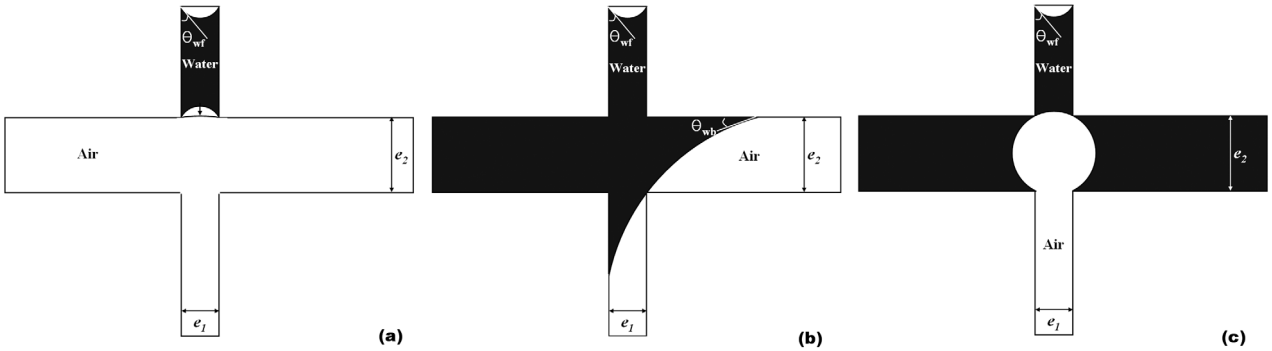

Figure 5. Idealized phase geometries (a) prior to the first entry into horizontal fractures; (b) prior to drainage after filling one horizontal fracture; and (c) prior to drainage after fully filling both of horizontal fractures in cases 0–2 for wetting flows.

the target intersection combined with a bigger horizontal fracture led to a longer hanging column, which will be discussed in the next section.

4. Analyses

[19] We conducted wetting/nonwetting invasion tests into the simple fracture intersections to explain the effects and the dynamics of intersection geometry on the phase structure at the intersection. Three cases, each having different fracture intersection conditions, were obtained and the results of them were compared with each other. Additionally, the viscous effects of the invader fluids on the pressures for the invader fluids to pass by the intersection and the phase structures at the intersection were observed.

4.1. Wetting Phase Flow

[20] From the results of the wetting phase flow tests, we were able to gain some critical observations: (1) Water was initially diverted into the horizontal fractures and then drained downward after obtaining sufficient pressure, which means that there are two CBs to breach at the fracture intersection between the vertical and horizontal fractures; (2) the pool heights at the first invasion into the horizontal fractures were similar, but the pool height for drainage into the lower vertical fracture were different in each case; and (3) the flow rate and the difference in apertures of the intersecting fractures affected the phase structure at the intersection.

[21] To analyze the dynamics of the invasion process of water into the air-filled simple fracture intersection, we will introduce capillary pressures in the fractures for wetting P_{cwf}, for draining P_{cdf}, in the CBs for wetting P_{cwb}, and for draining P_{cdb}. Considering the viscous pressure of water P_{vw}, the maximum gravity pressure $P_{g\max}$ to breach the intersection is given by

$$P_{g\max} \approx P_{cwb} - P_{cwf} - P_{vw}, \tag{1}$$

and from the Laplace-Young equation the maximum pool height to breach, $h_{p\max}$, is derived as

$$h_{p\max} \approx \frac{1}{\Delta\rho g}\left(-\frac{\sigma}{R_{wb}} + \frac{\sigma}{R_{wf}} - \frac{Q\mu L}{kA}\right), \tag{2}$$

where $\Delta\rho$ $[M/L^3]$ is the density difference between water and air, g $[L/T^2]$ is the acceleration due to gravity, σ $[M/T^2]$ is the interfacial tension between water and air, R_{wb} is the radius of the meniscus of air-water interface in the CBs for wetting of water, R_{wf} is the radius of the meniscus of air-water interface in fractures for wetting of water, Q $[L^3/T]$ is the injection rate of water, μ $[M/L \cdot T]$ is the dynamic viscosity of water, L $[L]$ is the distance back along the flow path from the intersection to the injection point, k $[L^2]$ is the permeability of the fracture, and A $[L^2]$ is the local cross-sectional area of the flow path.

[22] Figure 5a shows the process for water to invade the horizontal fractures. To breach the first CB that is located in the upper intersection corners, the meniscus should be flat and R_{wb} would be infinite to induce the film flow through edges of the horizontal fractures. Let us assume that the hysteresis comes from the different contact angle for wetting and draining, local aperture distribution, or in-plane curvature effects [*Glass et al.*, 2003], and then we can neglect the local aperture distribution and in-plane curvature at the intersection in these experiments. Then, R_{wf} is given by

$$R_{wf} = \frac{e_1}{2\cos\theta_{wf}}, \tag{3}$$

where, e_1 $[L]$ is the aperture of the vertical fracture (Figure 5a) and θ_{wf} is the contact angle in fractures for wetting of water. The estimated maximum pool heights to breach the first CB in the intersections at the flow rate of 0.012 mL/min are compared with the experimental results (Figure 3a). The dashed line is the estimated maximum pool heights from equations (2) and (3) from assumptions of pure water at 25°C and θ_{wf} of 50°, which is almost identical with the experimental results. As expected, these results are independent of e_2.

[23] In the ideal case where the fractures at the intersection match perfectly, water may invade both of the horizontal fractures, but there is likely to be an offset in the intersection which leads to the diversion of flow to one horizontal fracture. After filling one horizontal fracture, water invades the other horizontal fracture or drains into the lower vertical fracture, then R_{wb} will be the radius of the meniscus of air-water interface when the interface is in contact with the lower right corner of the intersection (Figure 5b):

$$R_{wb} = \frac{(e_1 + e_2)\cos\theta_{wb} + \sqrt{e_1^2 + e_2^2 - (e_1 - e_2)^2\cos^2\theta_{wb}}}{2\cos^2\theta_{wb} - 1}, \tag{4}$$

where, θ_{wb} is the contact angle in CBs for wetting of water and e_2 [L] is the aperture of the horizontal fracture (Figure 5b). Figure 3b shows the arithmetic mean of pool heights for the first drainage to the lower vertical fracture where water fills only one horizontal fracture at the flow rate of 0.012 mL/min. For comparison, the estimated maximum pool heights from equations (2)–(4) are also presented with the dashed curve that assumes θ_{wb} of 0°, which show a good agreement with the experimental results.

[24] If both of the horizontal fractures are fully filled with water, when the air-water interfaces in the horizontal and upper vertical fractures touch (Figure 5c), the second CB is breached, and water enters the intersection and the lower vertical fracture. R_{wb} will be given by

$$R_{wb} = \frac{\sqrt{e_1^2 + e_2^2}}{2}. \tag{5}$$

[25] When the pool height of water above the intersection reaches the maximum pool height, CBs in the intersection are breached and water goes down, passing through the intersection. If P_{cdb} is smaller than P_{cwf} of the vertical fracture beneath the intersection, the CBs remain open, and water still goes down until the pressure in the upper vertical fracture decreases below P_{cdf} [*Glass et al.*, 2003]. After the CBs are closed, the minimum gravity pressure $P_{g\min}$ that is the gravity pressure of water just after a breach will be given by

$$P_{g\min} \approx P_{cdb} - P_{cdf} - P_{vw}. \tag{6}$$

If we assume that water in the horizontal fractures contacts the CBs [*Glass et al.*, 2003], P_{cdb} equals the P_{cwf} of the horizontal fractures, equation (6) is changed to

$$P_{g\min} \approx P_{cwf} - P_{cdf} - P_{vw}, \tag{7}$$

and the minimum pool height, $h_{p\min}$, becomes

$$h_{p\min} \approx \frac{1}{\Delta\rho g}\left(-\frac{\sigma}{R_{wf}} + \frac{\sigma}{R_{df}} - \frac{Q\mu L}{kA}\right), \tag{8}$$

where, $R_{wf} = e_2/2\cos\theta_{wf}$, $R_{df} = e_1/2\cos\theta_{df}$, and θ_{df} is the contact angle in fractures for draining of water. Equation (8) is verified against the experiments (Figure 3c). The dashed line in Figure 3c is the estimated minimum pool heights at the flow rate of 0.012 mL/min under assumption of θ_{df} at 30°: There is a good agreement between the results estimated and those from the wetting flow experiments.

[26] Figures 6a–6c show the viscous effects of the injected water on maximum and minimum pool heights at the intersections of cases 0, 1, and 2. Solid triangles in Figure 6 are the means of observed maximum and minimum pool heights when only one horizontal fracture is filled with water, and open triangles are the means of them when both of horizontal fractures are filled with water. The experimental results are used for verification of our theoretical analyses: The solid lines in Figure 6 are the estimated maximum and minimum pool heights at the given flow rate using equations (2)–(4) and (8) when water fills only one horizontal fracture, while the dashed lines are the estimated maximum and minimum pool heights using equations (2), (3), (5), and (8) when both of horizontal fractures are filled with water. The comparison between the estimations from suggested equations and the observations from experiments suggests that our theoretical analyses can describe the capillary and viscous effects on wetting flow at a fracture intersection. The experimental and theoretical results propose that the viscous forces remain subordinate to capillary forces and are not enough to overcome the capillary effects at the intersection in our experimental scale when water fills only one horizontal fracture. However, if both of horizontal fractures are filled with water, the capillary effects are reduced and the viscous forces of water can make for water to cross the intersection without interruption.

4.2. Nonwetting Phase Flow

[27] Experimental observations gathered from the nonwetting phase flow tests can be summarized as follows: (1) TCE always invaded the intersections without interruption independently of the aperture variation in intersecting fractures; (2) invading TCE diverted into the horizontal fractures or drained downward without spreading out through the intersection; (3) the lengths of hanging TCE columns were different in each case; and (4) after the formation of a continuous tendril, the flow rate of TCE did not affect the phase structure.

[28] To analyze the dynamics of the invasion process of DNAPL into the water-filled simple fracture intersections, like the wetting flow, we need to quantify capillary pressures in the fracture for wetting P_{cnwf}, for draining P_{cndf}, in the intersection for wetting P_{cnwi}, and for draining P_{cndi}. The entry pressure into the intersection is given by the capillary and viscous pressures of DNAPL:

$$P_{entry} \approx P_{cnwi} - P_{cnwf} - P_{vn}, \tag{9}$$

and the entry pressure head of DNAPL into the intersection, h_{entry}, is followed:

$$h_{entry} \approx \frac{1}{\Delta\rho g}\left(-\frac{\sigma}{R_{nwi}} + \frac{\sigma}{R_{nwf}} - \frac{Q\mu L}{kA}\right), \tag{10}$$

where P_{vn} is the viscous pressure of DNAPL, $\Delta\rho$ [M/L^3] is the density difference between DNAPL and water, σ [M/T^2] is the interfacial tension between DNAPL and water, R_{nwi} is the radius of the meniscus of water-DNAPL interface in the intersection for wetting of DNAPL, R_{nwf} is the radius of the meniscus of water-DNAPL interface in fractures for wetting of DNAPL, Q [L^3/T] is the injection rate of DNAPL, and μ [$M/L \cdot T$] is the dynamic viscosity of DNAPL. In the intersection geometry like our experiments, we can neglect the in-plane curvature at the intersection. Then, when the interface touches all corners of the intersection (Figure 7), R_{nwi} can be defined as

$$R_{nwi} = -\frac{\sqrt{e_1^2 + e_2^2}}{2}, \tag{11}$$

and R_{nwf} is given by

$$R_{nwf} = \frac{e_1}{2\cos\theta_{nwf}}, \tag{12}$$

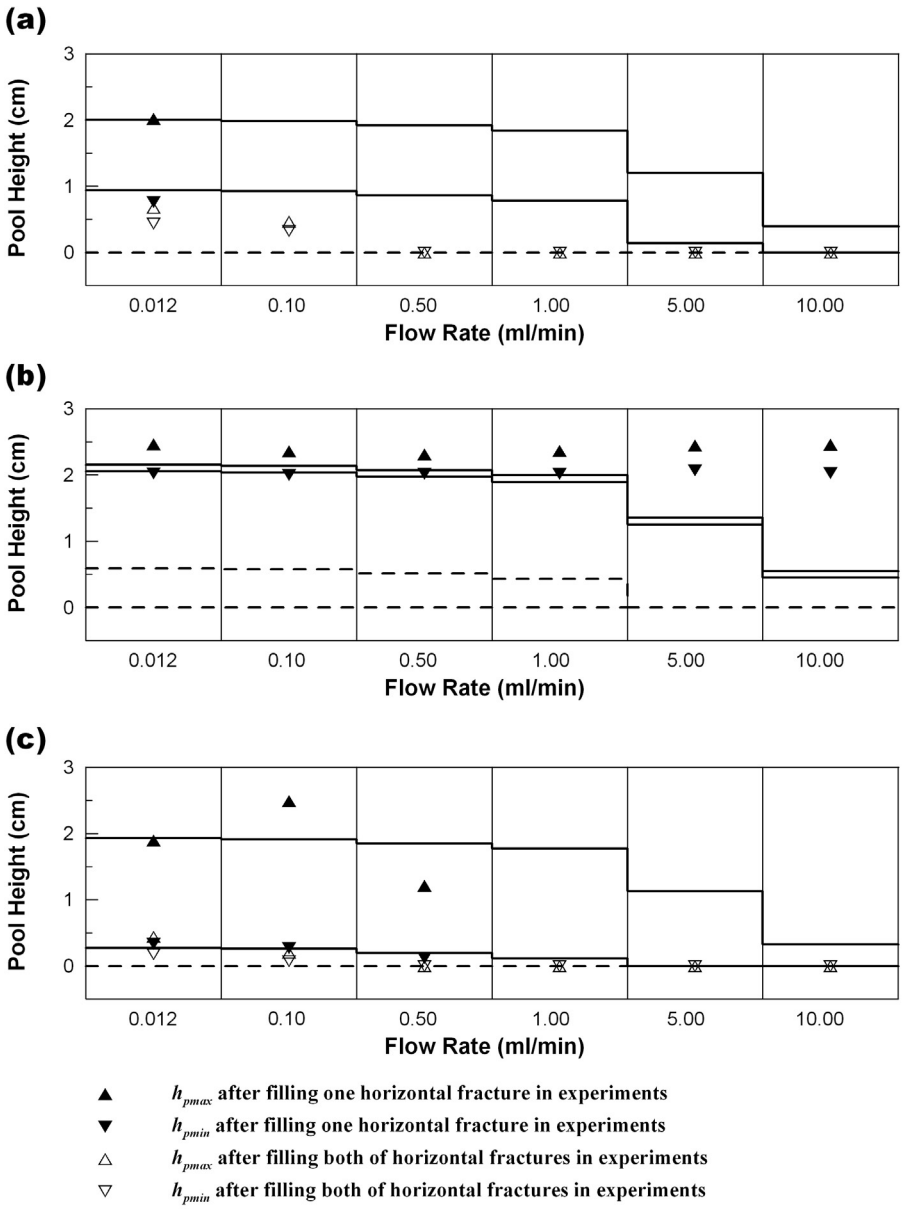

Figure 6. The effects of the water flow rate on maximum and minimum pool heights for (a) case 0, (b) case 1, and (c) case 2. The solid triangles are experimental results of maximum and minimum pool heights after filling only one horizontal fracture, and the open triangles are those of them after filling both of horizontal fractures. The solid lines are estimated maximum and minimum pool heights using equations (2)–(4) and (8), while the dashed lines using equations (2), (3), (5), and (10).

where θ_{nwf} is the contact angle in fractures for wetting of DNAPL. In our experimental conditions, h_{entry} into the intersection given by equations (10)–(12) has negative values, which means a DNAPL blob always invades the fracture intersection without interruption when it meets the intersection.

[29] After entrance of DNAPL to the intersection, DNAPL can move to the lower vertical or horizontal fractures, or spread out through the intersection. The migration path of DNAPL can be estimated using the invadability in the modified invasion percolation (MIP) model [*Meakin et al.*, 1992; *Xu et al.*, 1998; *Amundsen et al.*, 1999; *Ji et al.*, 2003]. The invadability is derived from the combination of capillary, gravity, and viscous pressures, so that

$$I = -P_c + P_g + P_{vi} - P_{vd}, \tag{13}$$

where I is the invadability of a invader fluid, P_c is the capillary pressure, P_g is the gravity pressure, P_{vi} is the viscous pressure of an invader fluid, and P_{vd} is the viscous pressure of a defender fluid. If DNAPL spread out through a fracture intersection, P_c in that direction becomes

$$P_c = \frac{4\sigma}{\sqrt{e_1^2 + e_2^2}}. \tag{14}$$

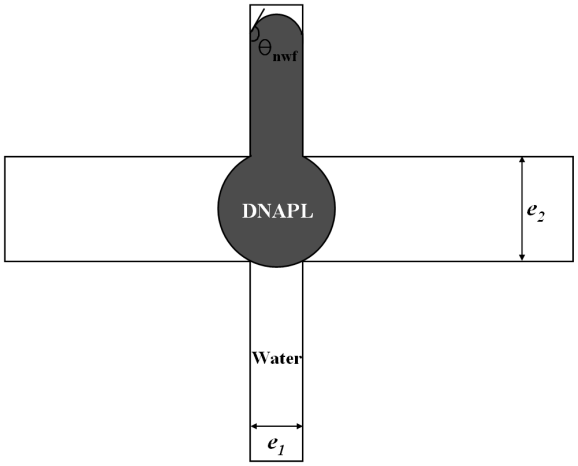

Figure 7. Idealized phase geometry when DNAPL invades a water-saturated intersection in cases 0–2 for nonwetting flows.

Then, when DNAPL goes to vertical or horizontal fractures from an intersection, P_c is given by

$$P_c = -\frac{\sigma}{R_c} = -\frac{2\sigma\cos\theta_{nwf}}{e_1 \text{ or } e_2}, \tag{15}$$

where R_c is the radius of the meniscus of water-DNAPL interface in vertical or horizontal fractures for wetting of DNAPL. Equations (13)–(15) explain well our observations: Invading TCE diverted into the horizontal fractures in case 1, and drained downward in cases 0 and 2, but did not spread out through the intersection.

[30] When DNAPL leaves the intersection for the lower vertical or horizontal fractures of capillary pressure P_c, the entry pressure is given by

$$P_{entry} \approx P_c - P_{cnwi} - P_{vn}, \tag{16}$$

and the entry pressure head of DNAPL becomes

$$h_{entry} = \frac{1}{\Delta\rho g}\left(-\frac{\sigma}{R_c} + \frac{\sigma}{R_{nwi}} - \frac{Q\mu L}{kA}\right), \tag{17}$$

where R_{nwi} and R_c are given by equations (11) and (15), respectively. Equation (17) cannot be established in this study because the length of TCE blobs in our tests (range ~1.1 to ~5.8 cm) is larger than the estimated entry pressure heads (range 0.12 to 1.39 cm). However, it could be verified indirectly from the experimental results: More TCE remained at the intersection after TCE drainage when the aperture of a horizontal fracture was larger (Figure 4).

[31] The viscous effects from the nonwetting phase flow rates on the entry pressure head could not be measured in the experiments, but can be inferred from the flow rate where TCE blobs change to continuous tendrils. Figure 8 shows estimated entry pressure heads from equation (17), and dots in Figure 8 are the arithmetic mean of flow rates where a tendril was formed below the intersection for each case. The flow rates where the estimated entry pressure head becomes zero are similar to those where a tendril was formed below the intersection considering the flow rate increased discretely in the tests. The estimated capillary effects in the intersection become subordinate to the viscous effect when the flow rate is sufficiently large like the wetting flow after filling both of horizontal fractures with water. However, note that the flow rate did not affect the phase structure near the intersection after formation of a continuous tendril in the experiments.

5. Concluding Remarks

[32] Our experiments and subsequent mathematical analyses demonstrate the substantial difference of the wetting and nonwetting flows at a simple intersection between horizontal and vertical fractures of different apertures. For wetting flows, two CBs existed at the entrance the intersection, which leads simple diversion and drainage of the wetting flow with impeding gravity-driven fingers within single fractures. However, a CB for nonwetting flows that is located on the exit from the intersection continues fingering as a capillary bridge and determines the nonwetting phase fluid migration path. For both wetting and nonwetting flows, the strengths of CBs at the intersection are determined by the combination of capillary and viscous pressures, and the differing aperture between intersecting fractures controls capillary pressure except the first CB for the wetting flow. Various phase geometries at wetting phase fluid flow vary the capillary effects from superior to coordinate to the viscous effects. However, the viscous effect on the nonwetting flow is coordinate to the capillary effect from the single phase geometry, and does not affect the phase structure near the intersection after formation of a continuous tendril.

[33] Projection of our results and analyses to a regular fracture network of vertical and horizontal fractures suggests substantial differences of phase structures of wetting and nonwetting flows. The continuous first breach by the wetting phase fluid to the horizontal fractures would always give rise to a slender-ladder phase structure despite the various geometric conditions at intersections. However, the network-scale phase structure of the nonwetting flows would be various depending on the given geometric con-

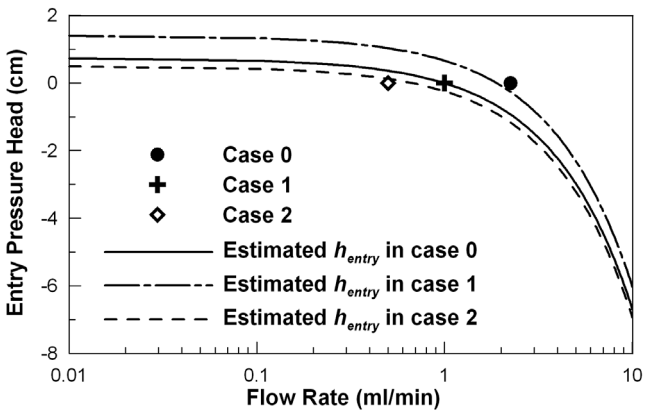

Figure 8. The effects of the TCE flow rate on formation of continuous tendrils. The lines are estimated entry pressure heads of TCE to the lower vertical fracture using equation (17), and the dots are the mean flow rates where a tendril was formed below the intersection for cases 0–2.

ditions at each intersection that determines the migration path; that is, the nonwetting phase fluid would simply go downward directly, merely spread laterally, or make a slender-ladder structure following the given geometric conditions at each intersection. In this point of view, the fracture intersection with differing aperture can be a more significant factor controlling the network-scale phase structure for the nonwetting than the wetting flows.

[34] Finally, natural fracture sets will have much larger degrees of freedom at intersections than our simple system: For example, individual fractures will have variable apertures, and their orientations will be various from the vertical and horizontal ones. Nevertheless, our results show the degree of change in void geometry between fracture and intersection affects the wetting and nonwetting flows differently, and its influence can be estimated quantitatively; which provides a stepping-stone in the expansion of our understanding of process and thus the characterization of the phase structure in natural fractured rocks.

[35] **Acknowledgments.** This study was supported by U.S. Department of Energy's Environmental Management Science Program under contact DE-AC04-94AL85000 at Sandia National Laboratories and DE-FG07-02ER63499 at the University of Idaho; the BK 21 project of the Korean Government; AEBRC of POSTECH; and the 21st Frontier project (Sustainable Water Resources Research Center 3-4-2). We would also like to acknowledge assistance from L. Orear in fabricating the experimental apparatus.

References

Amundsen, H., G. Wagner, U. Oxaal, P. Meakin, J. Feder, and T. Jossang (1999), Slow two-phase flow in artificial fractures: Experiments and simulations, *Water Resour. Res.*, *35*(9), 2619–2626.

Bahat, D., and T. Engelder (1984), Surface-morphology on cross-fold joints of the Appalachian Plateau, New York and Pennsylvania, *Tectonophysics*, *104*(3–4), 299–313.

Bird, R. B., W. E. Stewart, and E. N. Lightfoot (1960), *Transport Phenomena*, 780 pp., John Wiley, Hoboken, N. J.

Dragila, M. I., and N. Weisbrod (2004), Fluid motion through an unsaturated fracture junction, *Water Resour. Res.*, *40*, W02403, doi:10.1029/2003WR002588.

Glass, R. J., S. H. Conrad, and W. Peplinski (2000), Gravity destabilized nonwetting phase invasion in macroheterogeneous porous media: Experimental observations of invasion dynamics and scale analysis, *Water Resour. Res.*, *36*(11), 3121–3138.

Glass, R. J., M. J. Nicholl, A. L. Ramirez, and W. D. Daily (2002a), Liquid phase structure within an unsaturated fracture network beneath a surface infiltration event: Field experiment, *Water Resour. Res.*, *38*(10), 1199, doi:10.1029/2000WR000167.

Glass, R. J., M. J. Nicholl, S. E. Pringle, and T. R. Wood (2002b), Unsaturated flow through a fracture-matrix network: Dynamic preferential pathways in meso-scale laboratory experiments, *Water Resour. Res.*, *38*(12), 1281, doi:10.1029/2001WR001002.

Glass, R. J., M. J. Nicholl, H. Rajaram, and T. R. Wood (2003), Unsaturated flow through fracture networks: Evolution of liquid phase structure, dynamics, and the critical importance of fracture intersection, *Water Resour. Res.*, *39*(12), 1352, doi:10.1029/2003WR002015.

Hakami, E., and E. Larsson (1996), Aperture measurements and flow experiments on a single natural fracture, *Int. J. Rock Mech. Min. Sci. Geomech. Abstr.*, *33*(4), 395–404.

Ji, S.-H., I. W. Yeo, K. K. Lee, and R. J. Glass (2003), Influence of ambient groundwater flow on DNAPL migration in a fracture network: Experiments and simulations, *Geophys. Res. Lett.*, *30*(10), 1504, doi:10.1029/2003GL017064.

Ji, S.-H., M. J. Nicholl, R. J. Glass, and K. K. Lee (2004), Influence of a simple fracture intersection on density-driven immiscible flow: Wetting versus nonwetting flows, *Geophys. Res. Lett.*, *31*, L14501, doi:10.1029/2004GL020045.

Keller, A. (1998), High resolution, non-destructive measurement and characterization of fracture apertures., *Int. J. Rock Mech. Min. Sci.*, *35*(8), 1037–1050.

Kulander, B. R., C. C. Barton, and S. L. Dean (1979), The application of fractography to core and outcrop fracture investigations, *METC/SP-79/3*, 174 pp., Morgantown Energy Technol. Cent., U.S. Dep. of Energy, Morgantown, W. Va.

LaViolette, R. A., R. J. Glass, T. R. Wood, T. R. McJunkin, K. S. Noah, R. K. Podgorney, R. C. Starr, and D. L. Stoner (2003), Convergent flow observed in a laboratory-scale unsaturated fractured system, *Geophys. Res. Lett.*, *30*(2), 1083, doi:10.1029/2002GL015775.

Lee, J., J. M. Kang, and J. Choe (2003), Experimental analysis on the effects of variable apertures on tracer transport, *Water Resour. Res.*, *39*(1), 1015, doi:10.1029/2001WR001246.

Meakin, P., J. Feder, V. Frette, and T. Jossang (1992), Invasion percolation in a destabilizing gradient, *Phys. Rev. A*, *46*(6), 3357–3368.

Nicholl, M. J., and R. J. Glass (2002), Field investigation of flow processes associated with infiltration into an initially dry fracture network at Fran Ridge, Yucca Mountain, Nevada: A photo essay and data summary, *SAND2002-1369*, 75 pp., Sandia Natl. Lab., Albuquerque, N. M.

Weast, R. C. (Ed.) (1985), *CRC Handbook of Chemistry and Physics*, 66th ed., CRC Press, Boca Raton, Fla.

Wood, T. R., M. J. Nicholl, and R. J. Glass (2002), Fracture intersections as integrators for unsaturated flow, *Geophys. Res. Lett.*, *29*(24), 2191, doi:10.1029/2002GL015551.

Wood, T. R., R. J. Glass, T. R. McJunkin, R. K. Podgorney, R. A. LaViolette, K. S. Noah, D. L. Stoner, R. C. Starr, and K. Baker (2004), Unsaturated flow through a small fracture-matrix network: Part 1. Experimental observations, *Vadose Zone J.*, *3*, 90–100.

Wood, T. R., M. J. Nicholl, and R. J. Glass (2005), Influence of fracture intersections under unsaturated, low-flow conditions, *Water Resour. Res.*, *41*, W04017, doi:10.1029/2004WR003281.

Xu, B., Y. C. Yortsos, and D. Salin (1998), Invasion percolation with viscous forces, *Phys. Rev. E*, *57*(1), 739–751.

R. J. Glass, Flow Visualization and Processes Laboratory, Sandia National Laboratories, P.O. Box 5800, Albuquerque, NM 87185-1137, USA. (rjglass@sandia.gov)

S.-H. Ji, Department of Earth Sciences, University of Waterloo, 200 University Avenue West, Waterloo, Ontario, Canada N2L 3G1. (shji@scimail.uwaterloo.ca)

K.-K. Lee, School of Earth and Environmental Sciences, Seoul National University, Seoul 151–747, South Korea. (kklee@snu.ac.kr)

M. J. Nicholl, Geoscience Department, University of Nevada, 4505 Maryland Parkway, Las Vegas, NV 89122, USA. (michael.nicholll@ccmail.nevada.edu)